PNAS RESEARCH ARTICLE | MEDICAL SCIENCES

CFI-402257, a TTK inhibitor, effectively suppresses hepatocellular carcinoma

Cerise Yuen-Ki Chan[a,f], David Kung-Chun Chiu[a], Vincent Wai-Hin Yuen[a,f], Cheuk-Ting Law[a], Bowie Po-Yee Wong[a], Kelsie Lynn Thu[e], David Ward Cescon[e], Isabel Soria-Bretones[e], Jacinth Wing-Sum Cheu[a,f], Derek Lee[a,f], Aki Pui-Wah Tse[a,f], Misty Shuo Zhang[a,f], Kel Vin Tan[b], Irene Oi-Lin Ng[a,d], Pek-Lan Khong[b], Thomas Chung-Cheung Yau[c,d], Mark Robert Bray[e], Tak Wah Mak[e,f,1], and Carmen Chak-Lui Wong[a,d,f,1]

Contributed by Tak Mak; received October 26, 2021; accepted May 5, 2022; reviewed by Gen-Sheng Feng and Amaia (Amaya) Lujambio

Deregulation of cell cycle is a typical feature of cancer cells. Normal cells rely on the strictly coordinated spindle assembly checkpoint (SAC) to maintain the genome integrity and survive. However, cancer cells could bypass this checkpoint mechanism. In this study, we showed the clinical relevance of threonine tyrosine kinase (TTK) protein kinase, a central regulator of the SAC, in hepatocellular carcinoma (HCC) and its potential as therapeutic target. Here, we reported that a newly developed, orally active small molecule inhibitor targeting TTK (CFI-402257) effectively suppressed HCC growth and induced highly aneuploid HCC cells, DNA damage, and micronuclei formation. We identified that CFI-402257 also induced cytosolic DNA, senescence-like response, and activated DDX41-STING cytosolic DNA sensing pathway to produce senescence-associated secretory phenotypes (SASPs) in HCC cells. These SASPs subsequently led to recruitment of different subsets of immune cells (natural killer cells, $CD4^+$ T cells, and $CD8^+$ T cells) for tumor clearance. Our mass cytometry data illustrated the dynamic changes in the tumor-infiltrating immune populations after treatment with CFI-402257. Further, CFI-402257 improved survival in HCC-bearing mice treated with anti-PD-1, suggesting the possibility of combination treatment with immune checkpoint inhibitors in HCC patients. In summary, our study characterized CFI-402257 as a potential therapeutic for HCC, both used as a single agent and in combination therapy.

CFI-402257 | TTK inhibitor | STING pathway | cytosolic DNA sensing | senescence

Hepatocellular carcinoma (HCC), a malignancy originating from hepatocytes, is the fifth-most common cancer worldwide and accounts for 80% of primary liver cancers. Symptom presentation occurs at late stages for most HCC patients. Most patients are therefore not suitable for the most curative treatment, surgical resection or liver transplantation. HCC has a high recurrent rate and is refractory to conventional chemotherapies. The survival rate of HCC patients is only 10%, and HCC remains the second-most leading cause of cancer death worldwide. Sorafenib, lenvatinib, and combined treatment of bevacizumab (vascular endothelial growth factor [VEGF] inhibitor) and atezolizumab (immune checkpoint inhibitor [ICI] which targets programmed death-ligand 1 [PD-L1]) are currently the Food and Drug Administration (FDA)-approved targeted therapeutic agent for advanced HCC patients (1–4). However, these treatments prolong the lifespan of HCC patients for only 3–7 mo (2). Regorafenib and nivolumab (ICI targeting programmed death 1 [PD-1]) were approved by FDA as second-line treatments (5, 6). The effects of these targeted therapies are still far from satisfactory. Knowledge on the underlying molecular mechanisms in HCC is necessary for the advancement of effective therapeutic regimens for HCC patients.

Cancer genomes are unstable, and cancer cells have aberrant cell-cycle control allowing them to proliferate infinitely (7). Consequently, abnormal number of chromosomes, polyploidy (entire set of chromosomes) or aneuploidy (certain chromosomes), is found in 70–95% of human cancers (7). Abnormal chromosome number was traditionally believed to be a cause of cancer (7). However, cancer cells also acquire ability to endure poly/aneuploidy. The mitotic checkpoint, also called the spindle assembly checkpoint (SAC), ensures accurate chromosome segregation in mitosis. Targeting SAC proteins might result in high level of genomic instability and poly/aneuploidy to an extent even cancer cells could not tolerate causing senescence and apoptosis and thus is considered an attractive strategy against cancer (7). Multiple SAC proteins are frequently over-expressed in human cancers (7). The SAC proteins include BUBs, MADs, and threonine tyrosine kinase (TTK) which is also known as multipolar spindle 1 (MPS1) (8). TTK recruits other SAC proteins to unattached kinetochores in prometaphase to activate SAC-associated arrest (8). TTK-mediated SAC arrest is mainly

Significance

Hepatocellular carcinoma treatments available currently can only prolong the survival of patients for a few months and show a low response rate. Therapeutics that could provide more durable tumor suppression effect are needed. In this study, we characterized CFI-402257, a small molecule inhibitor targeting threonine tyrosine kinase (TTK), as a potential therapeutic drug in hepatocellular carcinoma. CFI-402257 disabled spindle assembly checkpoint, induced cytosolic DNA, activated stimulator of interferon genes (STING) pathway, and stimulated cytokines production in hepatocellular carcinoma cells, which would further promote anti-tumor immunity against hepatocellular carcinoma. Here, we demonstrate CFI-402257 is a potent therapeutic for hepatocellular carcinoma treatment, which targets hepatocellular carcinoma cells directly by inhibiting cell-cycle checkpoint functioning and indirectly by recruiting immune cells from the tumor-microenvironment.

Competing interest statement: T.W.M. and M.R.B. are co-founders and own stock in Treadwell Therapeutics. D.W.C. provides consultation for AstraZeneca, Exact Sciences, Eisai, Gilead, Novartis, GlaxoSmithKline, Merck, Pfizer, and Roche; has received grants from Inivata, GlaxoSmithKline, Merck, Pfizer, and Roche; and is the owner of patent US62/675,228. T.C.-C.Y. and A.L. are co-authors of guidelines article (doi:10.1136/jitc-2021-002794).

[1]To whom correspondence may be addressed. Email: tmak@uhnres.utoronto.ca or Tak.Mak@uhnresearch.ca or carmencl@pathology.hku.hk.

This article contains supporting information online at http://www.pnas.org/lookup/suppl/doi:10.1073/pnas.2119514119/-/DCSupplemental.

Published August 1, 2022.

through the inhibition of APC/C-CDC20 which would otherwise degrade securin and cyclin B to promote the progression of mitosis (8). Upregulation of TTK is found in bladder, thyroid, breast, lung, esophageal, and prostate cancers, as well as HCC (7, 9, 10). Upregulation of TTK is associated with poorer prognosis in glioblastoma (11). Inhibition of TTK resulted in cells with premature exit of mitosis with mis-segregated chromosomes (7). TTK inhibitors, NMS-P715 and MPI-0479605, suppressed the growth of ovarian and colorectal cancer xenografts in immune-deficient mice (12, 13); while another two TTK inhibitors, MPS-BAY2b and MPS-IN-3, synergized with anti-mitotic drugs paclitaxel and vincristine to inhibit growth of cervical cancer and glioblastoma xenografts in immune deficient mice (11, 14).

While a number of TTK inhibitors have entered clinical trials for advanced cancer patients (BAY 1161909, ClinicalTrials.gov identifier: NCT02138812; BAY 1217389, ClinicalTrials.gov identifier: NCT02366949), investigations on more specific TTK inhibitors with lower toxicity are actively underway. Recently, our drug discovery program for TTK inhibitors involving scaffold hopping exercise has identified an orally bioavailable TTK inhibitor, CFI-402257, with extremely high specificity, selectivity, and potency (15, 16). The TTK concentration that inhibits response by 50% (IC_{50}) and TTK K_i of CFI-402257 are 1.7 nM and 0.1 nM, respectively (15, 16). Cell-cycle analysis showed that CFI-402257 effectively induced polyploidy (8N and 16N) in HCT116 human colon cancer cells (15, 16). The growth inhibitory 50 (GI_{50}) of CFI-402257 in colon, ovarian, and breast cancer cells are 15 nM, 30 nM, and 160 nM, respectively (15, 16). CFI-402257 remarkably suppressed the growth of HCT116-derived colon cancer in immune deficient mice (16). Toxicology study showed that CFI-402257 has no signs of overt toxicity in rodents and dogs (16). Given the promising results of CFI-402257 in other preclinical cancer models, studies to evaluate its efficiency and efficacy in HCC are awaited.

Here, we characterized a highly potent and selective TTK inhibitor, CFI-402257, as a potential targeted therapy for HCC. TTK is overexpressed in human HCC. We hypothesized that targeting TTK would impair proper cell division and elevate poly/aneuploidy to an intolerable level that adversely halts HCC cell division and growth. Our data showed that TTK inhibitor would induce aneuploidy and senescence in HCC cells. The SASPs were elicited through DDX41-STING cytosolic DNA sensing pathway to promote tumor infiltrations of T cells, natural killer (NK) cells and other immune cells for tumor clearance. CFI-402257 also synergized with anti-PD-1 therapy to prolong survival. Our study will greatly facilitate the development of effective therapeutic regimens for HCC.

Results

TTK Overexpression Is Associated with Poor Prognosis in Human HCC. To understand the clinical relevance of TTK in human HCC, we evaluated the expressions of TTK in HCC tissues and their paired nontumorous liver (NT) tissues from the in-house HKU-QMH cohort at messenger RNA (mRNA) level by transcriptome sequencing (Fig. 1*A*) and quantitative real-time PCR (qPCR) (Fig. 1*B*). TTK was upregulated in 90% (54/60 cases) of the HCC patients by at least two-fold. The upregulation was further confirmed at the protein level by immunohistochemistry (IHC) (Fig. 1*C*). Transcriptome sequencing data of our HCC and NT tissues were subjected to Gene Ontology (GO) analysis. We examined the expression correlation between TTK and other genes by our in-house RNA sequencing (RNA-seq) data by Spearmen correlation analysis. GO analysis revealed that TTK coexpressed genes ($r < 0.6$) were significantly enriched in pathways involved in mitosis and cell division, suggesting a possible function of TTK in HCC (Fig. 1*D*). We further confirmed our study to a larger patient cohort from The Cancer Genome Atlas (TCGA) database. Consistently, TTK was significantly overexpressed (Fig. 1*E*) and high TTK expression was associated with poor overall and disease-free survival in human HCC (Fig. 1*F*). In addition, TTK was overexpressed in different solid tumor types, suggesting its importance in cancer progression (*SI Appendix*, Fig. S1). Further, OncoPrint analysis showed that TTK over-expression was the most significantly associated with mutations and deletions in TP53 and PTEN, the two commonly altered tumor suppressor genes and negative cell-cycle regulators (Fig. 1*G*). Higher TTK expression was also associated with poorer prognosis in TP53-mutated HCC cohort (*SI Appendix*, Fig. S2*A* and Table S1). In addition, overexpression of two other cell-cycle regulators (CDC20 and AURKA) showed the same result (*SI Appendix*, Fig. S2*B*).

TTK Promotes HCC Growth by Maintaining Proper Cell-Cycle Progression. To study the role of TTK in HCC development, we generated stable TTK knockdown clones in a luciferase-labeled human HCC cell line MHCC97L using short hairpin RNA (shRNA) knockdown approach (Fig. 2*A*). Knockdown of TTK induced chromosome mis-segregation as it functions as a SAC protein (17) and it would further increase DNA damage, as indicated by the marker γH2A.X in immunofluorescent staining (Fig. 2*B*). We implanted the TTK knockdown clones (sh12 and sh20) and the paired nontarget control (NTC) into BALB/cAnN-nu mice orthotopically and NOD-SCID mice by tail vein injection. TTK knockdown significantly reduced tumor sizes in vivo (Fig. 2*C*) and incidence of lung metastasis (Fig. 2*D*).

CFI-402257 is an orally active, highly selective small molecule inhibitor for Mps1/TTK (18), and it is currently in phase 2 clinical trial for advanced solid tumors (ClinicalTrials.gov identifier: NCT02792465). CFI-402257 suppressed HCC cell proliferation dose-dependently (Fig. 2*E*) and induced HCC apoptosis (Fig. 2*F*). Further, we observed that HCC cell lines (Hep3B, Huh7, MHCC97L, PLC/PRF/5, and Hepa1-6) were more sensitive to CFI-402257 than normal hepatocytes (MIHA), as indicated by their lower GI_{50} values (Fig. 2*G*). We profiled the chromosome content in HCC cells cultured with CFI-402257, and TTK inhibition led to increased proportion of cells with aneuploids in MHCC97L (Fig. 2*H*) and other HCC cell lines (*SI Appendix*, Fig. S3). A majority of the CFI-402257-treated cells showed ploidy at >2N and >4N level. Taken together, TTK promoted HCC growth by regulating proper cell-cycle propagation and ensuring chromosome segregation fidelity.

CFI-402257 Effectively Suppresses HCC Growth and Metastasis In Vivo. We further investigated the therapeutic potential of CFI-402257 using different mouse HCC models. We implanted MHCC97L in BALB/cAnN-nu mice orthotopically. After 2 wk of implantation when tumors were formed, CFI-402257 or vehicle control (Ctrl) was administered to mice orally. Notably, TTK inhibition by CFI-402257 shrank HCC tumors (Fig. 3*A* and *SI Appendix*, Fig. S4 *A–C*) and reduced lung metastasis (Fig. 3*B*). Previously, we identified TTK over-expression is closely associated with TP53 mutation/deletion in human HCC. To generate a mouse model that resembles the genetic makeup of human HCC, we introduced CRISPR/Cas9 system to knockout *Trp53* and a transposon system expressing *C-Myc* into immunocompetent

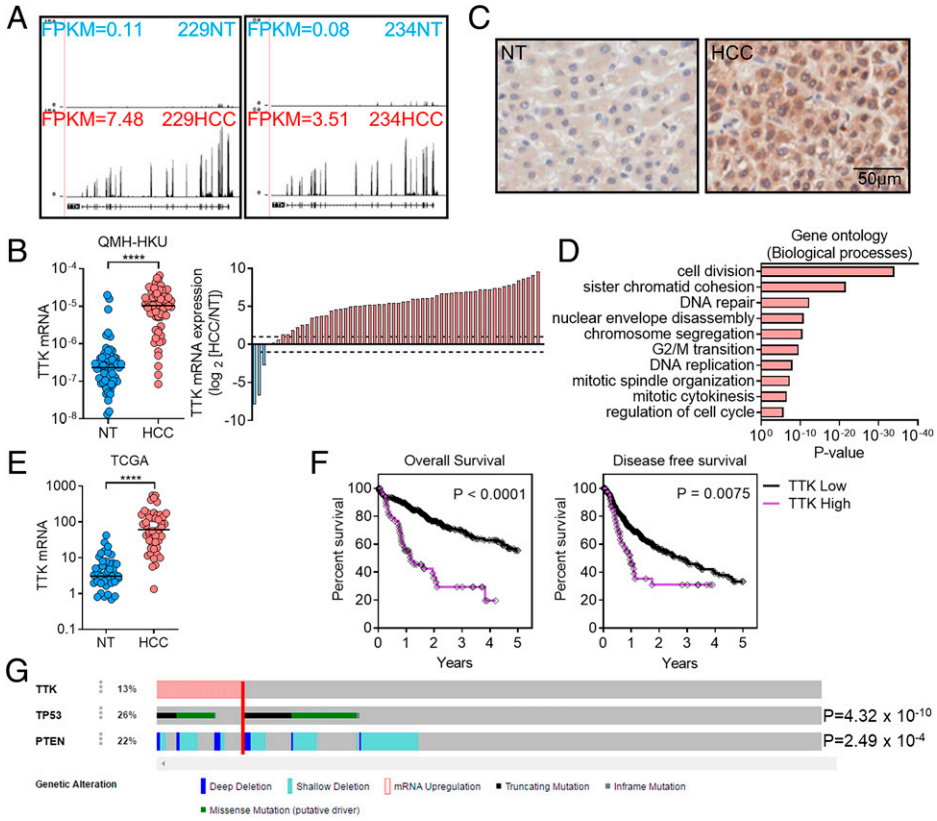

Fig. 1. Clinical significance of TTK upregulation in human HCC. (*A*) Representative pictures of raw aligned sequencing read obtained from transcriptome sequencing comparing TTK mRNA expression in HCC and the corresponding NT tissues of our cohort of patients (HKU-QMH). FPKM, fragments per kilobase of exon per million reads. (*B*) *Left*: TTK mRNA expression in 60 cases of paired HCC and NT tissues was evaluated by RT-qPCR. TTK mRNA expression is calculated based on the following equation: 2^ – (CT_{TTK} – CT_{18S}). *Right*: Waterfall plot showed that TTK expression was upregulated in 54/60 (90%) of HCC patients by at least twofold. Patients were from the HKU-QMH cohort. (*C*) TTK protein expression in a representative case of HCC and the corresponding NT tissues. (*D*) GO study using our in-house transcriptome sequencing data showed that TTK upregulation was associated with enrichment of pathways involved in mitosis and cell division. (*E*) TCGA database showed that TTK was over-expressed in 49 HCC patients. (*F*) TCGA database revealed that TTK upregulation was correlated with shorter overall and disease-free survival. Patients with TTK mRNA expression >1 SD of TTK mean value in HCC tissues were categorized into TTK high group. Survival curves were plotted based on the TTK mRNA values from over 300 HCC patients in TCGA database. (*G*) High TTK expression was associated with p53 or PTEN mutations and deletions in >400 HCC patients from TCGA. (*B*, *E*, and *G*) Paired *t* test, F-Kaplan Meier, and log-rank test. **P* < 0.05, ***P* < 0.01, ****P* < 0.001, *****P* < 0.0001.

C57BL/6 mice through hydrodynamic tail vein injection (HDTVi) (*SI Appendix*, Fig. S4 *D* and *E*). After 3 wk when the tumors were formed post-HDTVi (19), we administered the mice with CFI-402257 or Ctrl. After 17 d of treatment, mice were subjected to a magnetic resonance imaging (MRI) scan which showed a significant shrinkage of tumors (Fig. 3*C* and *SI Appendix*, Fig. S4*F*). After 21 d of treatment, we killed the mice and clearly confirmed that CFI-402257 significantly reduced the size of $Trp53^{KO}/Myc^{OE}$ HCC tumors (Fig. 3*D*) without adverse toxicity, as shown by no significant change in the body weight and hematoxylin/eosin staining of liver tissues (*SI Appendix*, Fig. S4 *G* and *H*).

In conjunction, we established stable TP53 knockdown MHCC97L clones and observed that TP53-knockdowns sensitized HCC cells toward CFI-402257 inhibition, suggesting rationale for using CFI-402257 in human HCC with TP53 mutations (*SI Appendix*, Fig. S5). Collectively, these data indicated that CFI-402257 is a potent suppressor of HCC tumor in vivo.

CFI-402257 Induces Senescence-like Response and SASP Secretion in HCC. Inhibition of TTK by CFI-402257 induced aneuploidy after abolishing SAC protection resulting in chromosome mis-segregation. By deactivating SAC, the kinetochore–microtubule attachment during mitosis is unchecked, and the emergence of unattached kinetochores leads to unequal chromosome segregation and formation of micronuclei (20, 21). Nuclear staining revealed the formation of micronuclei in human HCC cells after CFI-402257 treatment (Fig. 4*A*). Further, CFI-402257 treatment increased DNA damage, another consequence of lacking a functional SAC (17), thus echoing the effect of TTK knockdown as shown previously (Fig. 4*B*). CFI-402257 triggered micronuclei formation by disrupting chromosome segregation process. Furthermore, the nuclear envelop of micronuclei is vulnerable to rupture and therefore causes leakage of double-stranded DNA to cytosol, activating cellular DNA sensing pathway (22, 23). We found that CFI-402257 also increased cytosolic DNA in HCC cells (Fig. 4*C*). We hypothesized that the loss of tension at kinetochores for chromosome biorientation at mitosis, together with accumulation of irreparable DNA damage would lead to senescence. To substantiate our hypothesis, we assayed the senescence-like response in HCC cells by senescence-associate-β-galactosidase staining and found that CFI-402257 induced senescence broadly (Fig. 4*D*). The expressions of CCL2, interleukin (IL)-1α, and IL-1β, the representative senescence-associated secretory phenotype (SASP) markers, were upregulated by CFI-402257 (*SI Appendix*, Fig. S6 *A*–*C*). Increased secretions of CCL2 and IL-1β were observed in cells treated with CFI-402257 (Fig. 4*E*). To profile the expressions of SASP more comprehensively, transcriptome sequencing was performed. The result identified that expressions of 76/104

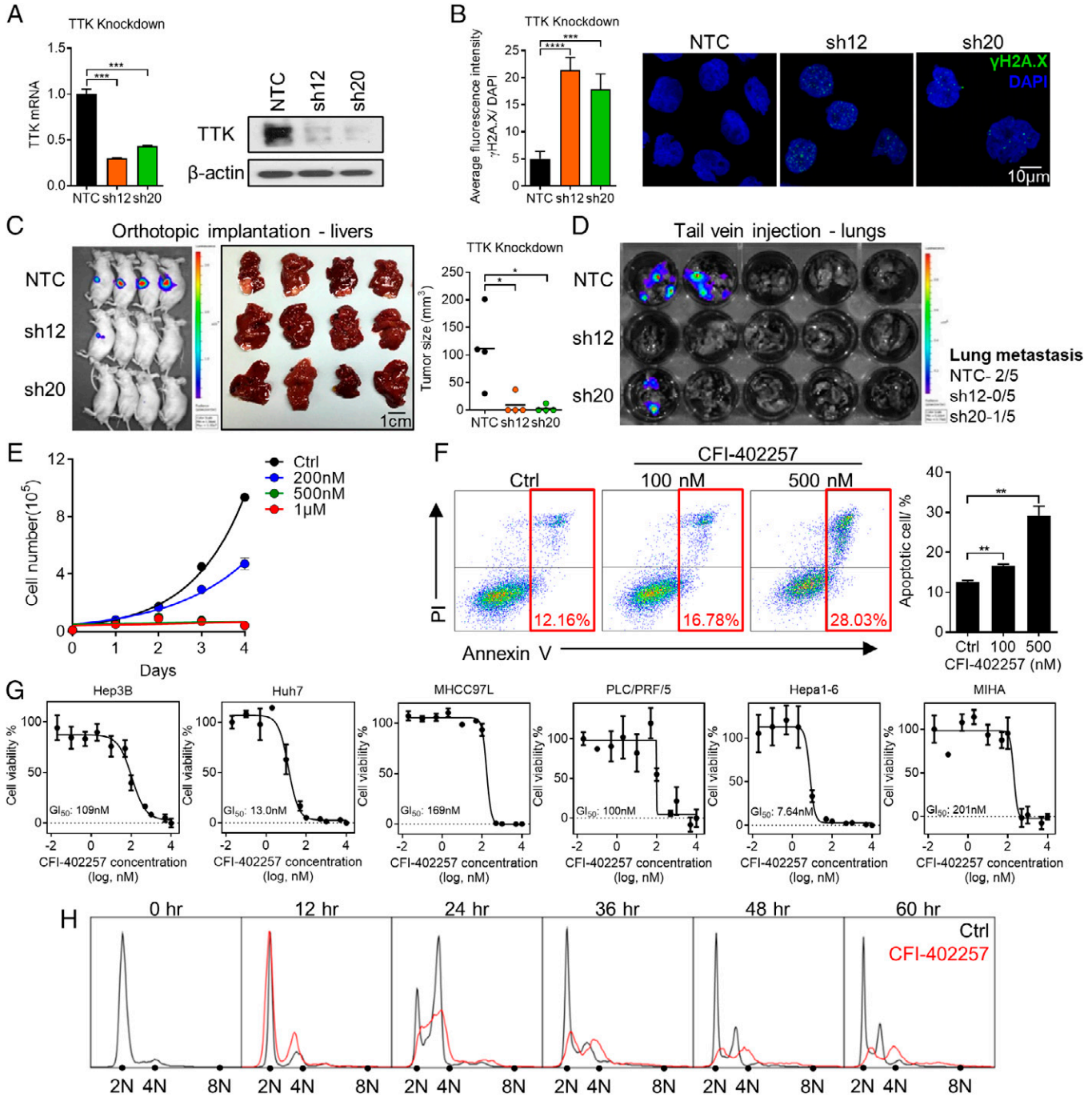

Fig. 2. Knockdown (KD) of TTK and CFI-402257, a TTK inhibitor, suppressed HCC growth. (*A*) Establishment of TTK-KD cells in MHCC97L using shRNA approach. RT-qPCR and Western blots showed the KD efficiency of MHCC97L cells expressing shRNAs targeting TTK or nontarget control (NTC). (*B*) Immunofluorescent imaging of TTK-KD cells in MHCC97L. Blue, DAPI; green, γH2A.X. (*C*) Luciferase-labeled TTK-KD and control MHCC97L cells were inoculated into the livers of BALB/cAnN-nu mice. *Left*: mice were subjected to Xenogen imaging. *Right*: livers were harvested and tumor size was measured by caliper. (*D*) Luciferase-labeled TTK-KD and control MHCC97L cells were injected into NOD-SCID mice through tail-veil. Lungs were harvested for ex vivo imaging for lung metastases. (*E*) MHCC97L cells were treated with escalating doses of CFI-402257 or vehicle control (Ctrl). Cell numbers were recorded daily. (*F*) MHCC97L cells were treated with 100 nM and 500 nM CFI-402257, a TTK inhibitor, or Ctrl for 48 h and subjected to Annexin V and propidium iodide (PI) staining. (*G*) XTT assay was performed with different doses of CFI-402257 for 5 d in a panel of HCC cell lines and a normal hepatic cell line, MIHA. GI_{50} was determined. (*H*) MHCC97L cells were synchronized by double thymidine treatment at G1 phase (0-h timepoint). Cells were released in the presence of 1 μM CFI-402257 or Ctrl at different time points. Cell-cycle profiles were determined by PI staining. Student's *t* test. $^{*}P < 0.05$, $^{**}P < 0.01$, $^{***}P < 0.001$, $^{****}P < 0.0001$.

SASP genes (24) were induced by CFI-402257, and data of the top 29 significantly upregulated genes were shown, including the markers we mentioned (Fig. 4*F* and *SI Appendix*, Fig. S6*C*). The induction of senescence and SASP genes were also validated in vivo (*SI Appendix*, Fig. S6*D*). To further test if cytosolic DNA is important for the upregulation of SASPs, we first generated stable clones overexpressing a cytoplasmic DNase named 3′ repair exonuclease 1 (TREX1) (MHCC97L-dCas9-sg2 and sg3) and the paired empty vector (ev) control (MHCC97L-dCas9-ev) (25) in HCC cells using CRISPR activation (CRISPRa) system. Accordingly, overexpression of TREX1 suppressed CFI-402257-induced CCL2 expression, at both mRNA and protein level (*SI Appendix*, Fig. S7), evidencing the presence of cytosolic DNA elicited SASP response. Our data converged to demonstrate that CFI-402257

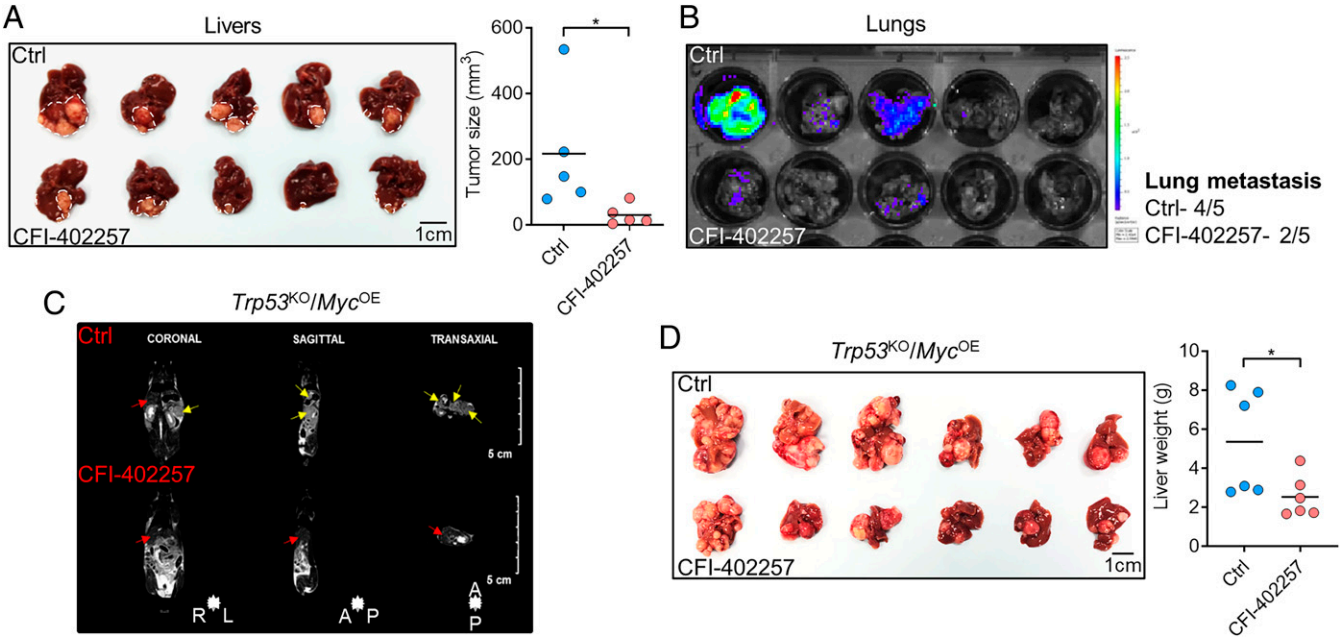

Fig. 3. Effects of TTK inhibitor in vivo. (*A* and *B*) BALB/cAnN-nu mice were orthotopically implanted with luciferase-labeled MHCC97L cells for 2 wk and were administered with vehicle control (Ctrl) or 6 mg/kg/day CFI-402257 for 19 d. (*A*) Livers were harvested for tumor size measurement. (*B*) Xenogen imaging of lungs harvested. (*C* and *D*) C57/BL6 mice were injected with transposon carrying *c-Myc* and CRISPR-Cas9 system targeting *Trp53* to over-express an oncogene and knock out a tumor suppressor gene through hydrodynamic tail vein injection (HDTVi). Mice were administered with Ctrl or 6 mg/kg/day CFI-402257 21 d postinjection for 21 d. (*C*) Mice were imaged by micro-MRI after 17 d of CFI-402257 treatment before sacrificing. Red arrows, liver tissue; yellow arrows, tumors. (*D*) Livers were harvested and weighed. Student's *t* test. $*P < 0.05$, $**P < 0.01$, $***P < 0.001$, $****P < 0.0001$.

treatment abolished SAC, leading to DNA damage, micronuclei formation, cytosolic DNA accumulation, and senescence-like response in HCC.

CFI-402257 Triggers SASP Transcription via DDX41–STING–IRF3/7–Nuclear Factor κB Axis. Micronuclei formation and cytosolic DNA accumulation would stimulate the STING pathway (22) which might be induced by CFI-402257. STING is a key regulator of cytosolic DNA sensing pathways that mediate proinflammatory cytokines signals upon stimulation by cytosolic DNA (26). STING is activated when cytosolic DNA is sensed by several sensors including DDX41, IFI16, and cGAS (26). Activated STING in dimerized form would then translocate from endoplasmic reticulum to Golgi, where it was palmitoylated and phosphorylated by TBK1. The STING-TBK1-IRF3 complex led to phosphorylation, dimerization and nuclear translocation of IRF3. The complex also phosphorylated IκB, causing nuclear translocation of nuclear factor κB (NF-κB). Eventually, transcription of interferon-stimulated genes (ISGs) and SASPs were activated (27). We confirmed activation of STING and its downstream mediator IRF3 as there were increased phosphorylation of these proteins in cells cultured with CFI-402257 (Fig. 5 *A* and *B*), as well as increased formation of dimerized STING (Fig. 5*C*). To investigate if STING-mediated DNA sensing pathway (27, 28) contributes to the SASP upregulation, we evaluated two representative SASP genes in stable knockdown clones of DDX41, STING, IRF7, and RelA (a subunit of NF-κB). Remarkably, knockdown of members in the STING pathway resulted in suppression of mRNA expression (*SI Appendix*, Fig. S8) and secretion of CCL2 and IL-1β (Fig. 5 *D* and *E*) after CFI-402257 treatment. In addition, our transcriptome sequencing data with STING stable knockdown clone (sh28) and NTC demonstrated the upregulation of a panel of SASPs upon CFI-402257 treatment was abrogated when STING was knocked down (Fig. 5*F*). Our data converged to show that CFI-402257 regulates SASP expression through DDX41–STING–IRF3/7–NF-κB axis in HCC cells.

Mass Cytometry Analysis Demonstrated Increase of Immune Cell Infiltration in HCC Tumor upon CFI-402257 Treatment. Previously, we showed CFI-402257 elicited SASP expression and secretion from HCC cells through activation of STING pathway and significantly suppressed HCC growth in vivo. The chemokines and cytokines of these SASPs can alter the number of infiltrating immune cells and their functional status in the tumor microenvironment (TME) and hence influence the clinical outcomes of targeted therapies (29). Therefore, mass cytometry, or cytometry by time of flight (CyTOF), which enabled us to simultaneously stain a larger panel of markers than conventional flow cytometry, was used to extensively classify the infiltrated immune populations in $Trp53^{KO}/Myc^{OE}$ background tumor (30). Our antibody panel comprised 10 markers for categorization of major immune cell lineages, and 30 markers for stratifying tumor-infiltrating T cells and NK cells by their activation, differentiation, mobilization and exhaustion states (e.g., KLRG1, PD-1, TIGIT, TIM3, and LAG3) (19). We simultaneously analyzed the expression of all the 40 markers on immune cells in HCC tumors in mice given or not given CFI-402257 treatment.

To have an overview on the change of tumor-infiltrating immune populations, we analyzed the samples with uniform manifold approximation and projection (UMAP) dimension reduction and overlaid the plots of vehicle control (Ctrl) and CFI-402257-treated mice to visualize the distribution of $CD45^+$ leukocytes on a two-dimensional map (Fig. 6*A* and *SI Appendix*, Fig. S9). We also analyzed with flow cytometry gating method to calculate the size of each population (Fig. 6*B* and *SI Appendix*, Fig. S10). The results showed that $CD4^+$ T cell, $CD8^+$ T cell, and NK cell populations were increased, and the regulatory T cell (Tregs) population was decreased after CFI-402257 treatment.

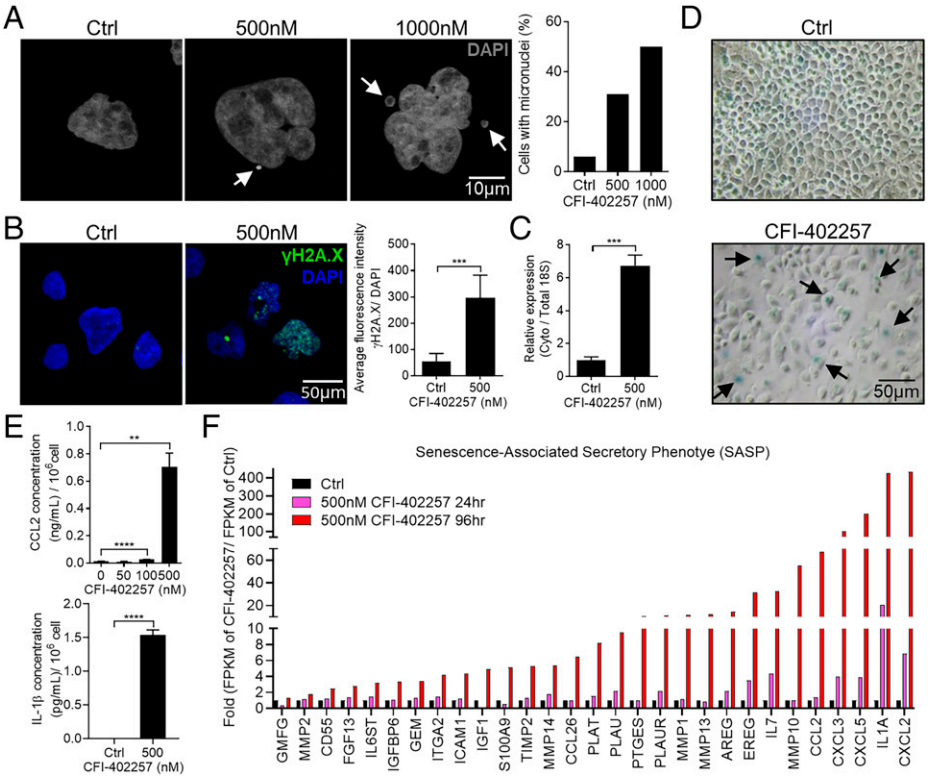

Fig. 4. TTK inhibitor induced micronuclei, cytosolic DNA, senescence, and SASP secretion in HCC cells. (*A*) MHCC97L cells were treated with different concentrations of CFI-402257 for 48 h and stained with DAPI for DNA staining. *Left*: representative images of micronuclei, indicated by arrows. *Right*: percentage of cells with micronuclei. (*B*) Immunofluorescent imaging of MHCC97L cells treated with 500 nM CFI-402257 and Ctrl for 48 h. Blue, DAPI; green, γH2A.X. (*C*) Quantification of cytosolic DNA in MHCC97L treated with 500 nM CFI-402257 and Ctrl for 48 h. (*D*) β-galactosidase assay was performed in MHCC97L cells treated with 2 μM CFI-402257 and Ctrl for 72 h. Senescent cells are indicated by arrows. (*E*) CCL2 and IL-1β protein expression was quantitated by ELISA and normalized to standard curve and cell number after treatment of the indicated concentrations of CFI-402257 for 96 h. (*F*) Transcriptome sequencing was performed in MHCC97L cells treated with 500 nM CFI-402257 at different time points. A total of 29 SASP genes that were dramatically upregulated were listed. Student's *t* test. $^{*}P < 0.05$, $^{**}P < 0.01$, $^{***}P < 0.001$, $^{****}P < 0.0001$.

To have a deeper understanding of the change in the immune populations and the subtypes present, we used phenograph to cluster $CD45^+$ leukocytes by unsupervised nearest neighbors grouping of parameters. A total of 23 clusters were identified (Fig. 6 *C* and *D* and *SI Appendix*, Fig. S11). Interestingly, we noted there were four clusters of NK cells and four clusters of $CD8^+$ T cells. Most of these clusters generally underwent an expansion, resembling the result from flow cytometry gating method. The general increase of NK cells in tumors from CFI-402257-treated mice suggested that NK cells might play a significant role in modulating the treatment efficacy. Although the alteration of functional status of NK cells was not obvious after CFI-402257 treatment, the abundance and diversity of NK cells suggested their potential role in controlling tumor size (*SI Appendix*, Fig. S12).

We further validated the dynamic change observed in the major immune populations by flow cytometry and IHC staining, consistently, the lymphoid populations were increased ($CD4^+$ T, $CD8^+$ T, and NK cells) only in HCC (T) but not nontumor (NT) regions (Fig. 6 *E*–*G* and *SI Appendix*, Fig. S13). To conclude, our immune cell profiling data suggested that CFI-402257 promoted anti-tumor immunity.

Mass Cytometry Analysis Demonstrated Upregulation of PD-1 in TIL in HCC Tumor upon CFI-402257 Treatment. We identified T cells as the major population presented in HCC tumors and it was largely increased after CFI-402257 treatment. T cells played a central role in cancer immunity (31, 32). To extend our understanding on the population change upon CFI-402257 treatment, we used the same approach for total leukocytes analysis above (UMAP and phenograph) to analyze T cells (*SI Appendix*, Fig. S14 *A* and *B*). We observed an increase in cluster 2 ($CD8^+$ T effector memory), and a decrease in clusters 1, 5, and 9 ($CD4^+$ T effector memory and $CD8^+$ T central memory) (*SI Appendix*, Fig. S14*C*). The expression levels of all T cell markers on UMAP plot, and the location of clusters on phenograph were clarified (*SI Appendix*, Figs. S15 and S16). To compare the activity of T cells in CFI-402257-treated and control mice, we gated the $CD4^+$ T and $CD8^+$ T effector memory cells and evaluated the expression of different functional markers, including granzyme B (GZMB), ICOS, OX40, PD-1, CTLA4, and TIGIT (33). The comparison showed no general upregulation of these activation or exhaustion markers, but it was noted that the expression of PD-1 is upregulated upon CFI-402257 treatment (*SI Appendix*, Figs. S17 and S18), providing rationale for combination therapy with anti-PD-1 to improve the efficiency of CFI-402257.

CFI-402257 Mediates Anti-Tumor Effects Partially through STING and Synergizes with Immune Checkpoint Inhibitor. To validate that STING is important for the effect of CFI-402257 in vivo, we established $Sting^{WT/KO}$ HCC tumors in mice and treated them with vehicle control (Ctrl) or CFI-402257. Noticeably, we observed knockout of STING diminished the survival benefit of CFI-402257. By comparing the median days of survival between Ctrl and CFI-402257-treatment groups, we saw CFI-402257 promoted longer survival in $Sting^{WT}$ group

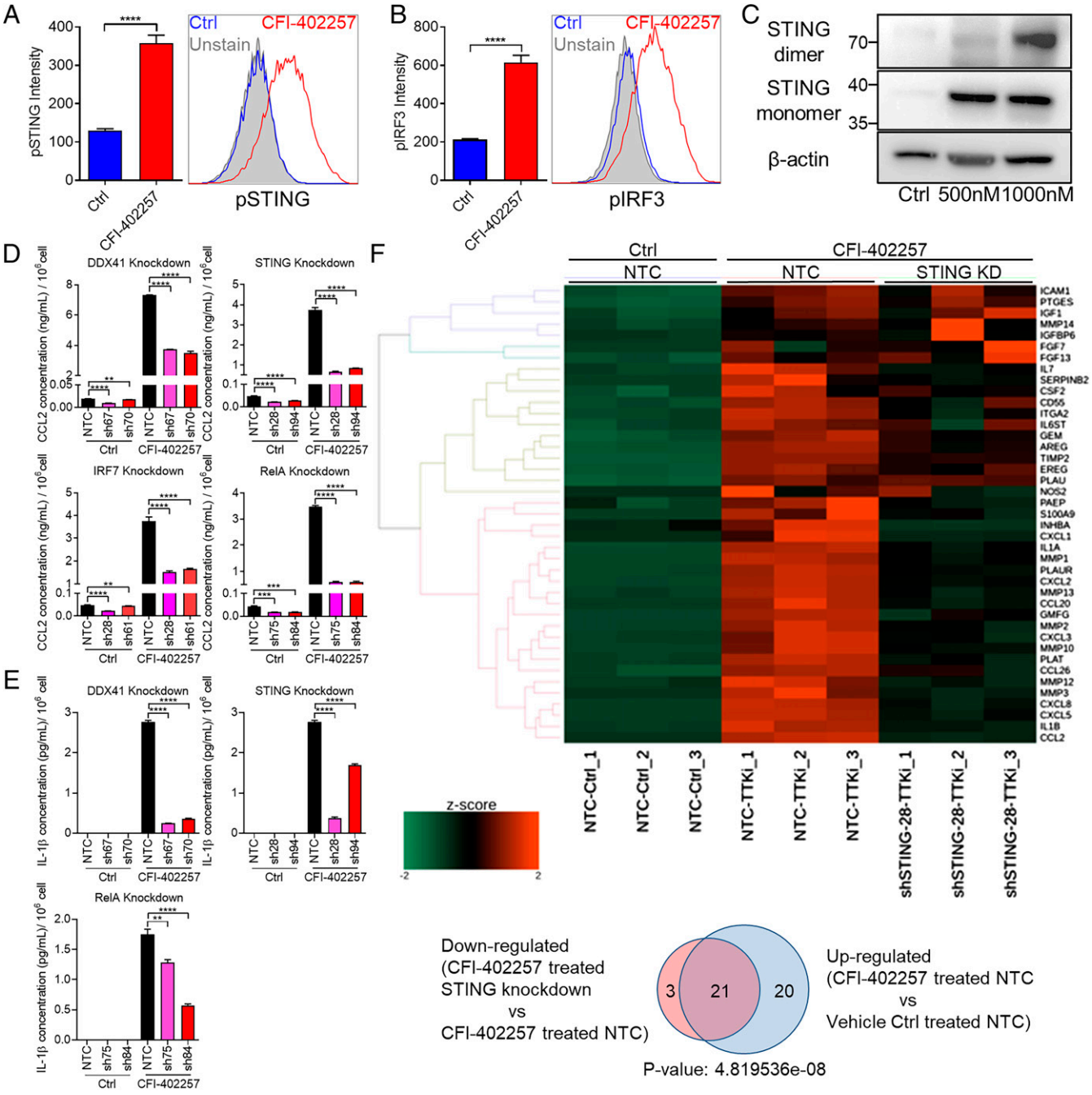

Fig. 5. TTK inhibitor regulated SASP expression through DDX41–STING–IRF3/7–NF-κB axis. (*A* and *B*) Phosphorylation status of (*A*) STING and (*B*) IRF3 after 500 nM CFI-402257 treatment in MHCC97L cells for 96 h. (*C*) Western blot showing STING dimer formation after 96 h of CFI-402257 treatment. (*D* and *E*) CCL2 and IL-1β protein expression in DDX41, STING, IRF7, and RelA stable knockdown MHCC97L cells treated with 500 nM CFI-402257 for 96 h. (*D*) CCL2. (*E*) IL-1β. (*F*) Transcriptome sequencing was performed in MHCC97L STING knockdown (KD) clone (sh28) and NTC treated with 500 nM CFI-402257 for 96 h. *Upper*: heatmap representing SASP expression data. *Lower*: GSEA of SASP expression data. (*A*, *B*, *D*, and *E*) Student's *t* test. (*F*) Fisher's exact test. $*P < 0.05$, $**P < 0.01$, $***P < 0.001$, $****P < 0.0001$.

(58 d vs. 110 d), but not in $Sting^{KO}$ group (61 d vs. 68 d) (Fig. 7*A* and *SI Appendix*, Fig. S19*A*).

To examine whether combination therapy of CFI-402257 with anti-PD-1 can enhance the treatment benefit of CFI-402257, we induced $Trp53^{KO}/Myc^{OE}$ HCC in mice by HDTVi and subjected them to treatment with Ctrl, CFI-402257 alone (released after 14 d of treatment), anti-PD-1 monoclonal antibody (mAb) alone or CFI-402257 and anti-PD-1 mAb. Excitingly, we observed the combination of CFI-402257 and anti-PD-1 mAb extended survival of HCC-bearing mice (Fig. 7*B* and *SI Appendix*, Fig. S19*B*).

Discussion

In this study, we reported the potent anti-tumor effect of CFI-402257, an orally available small molecule inhibitor which selectively targets TTK, in HCC model. When used as a single agent, CFI-402257 inhibited tumor growth by inducing apoptosis and senescence-like response. The DDX41-STING cytosolic DNA sensing pathway was activated in the senescent HCC cells and it promoted anti-tumor immune response through the upregulation and increased secretion of SASP, as revealed by mass cytometry and transcriptome sequencing (Fig. 7*C*). Combination treatment of CFI-402257 with anti–PD-1, an immune

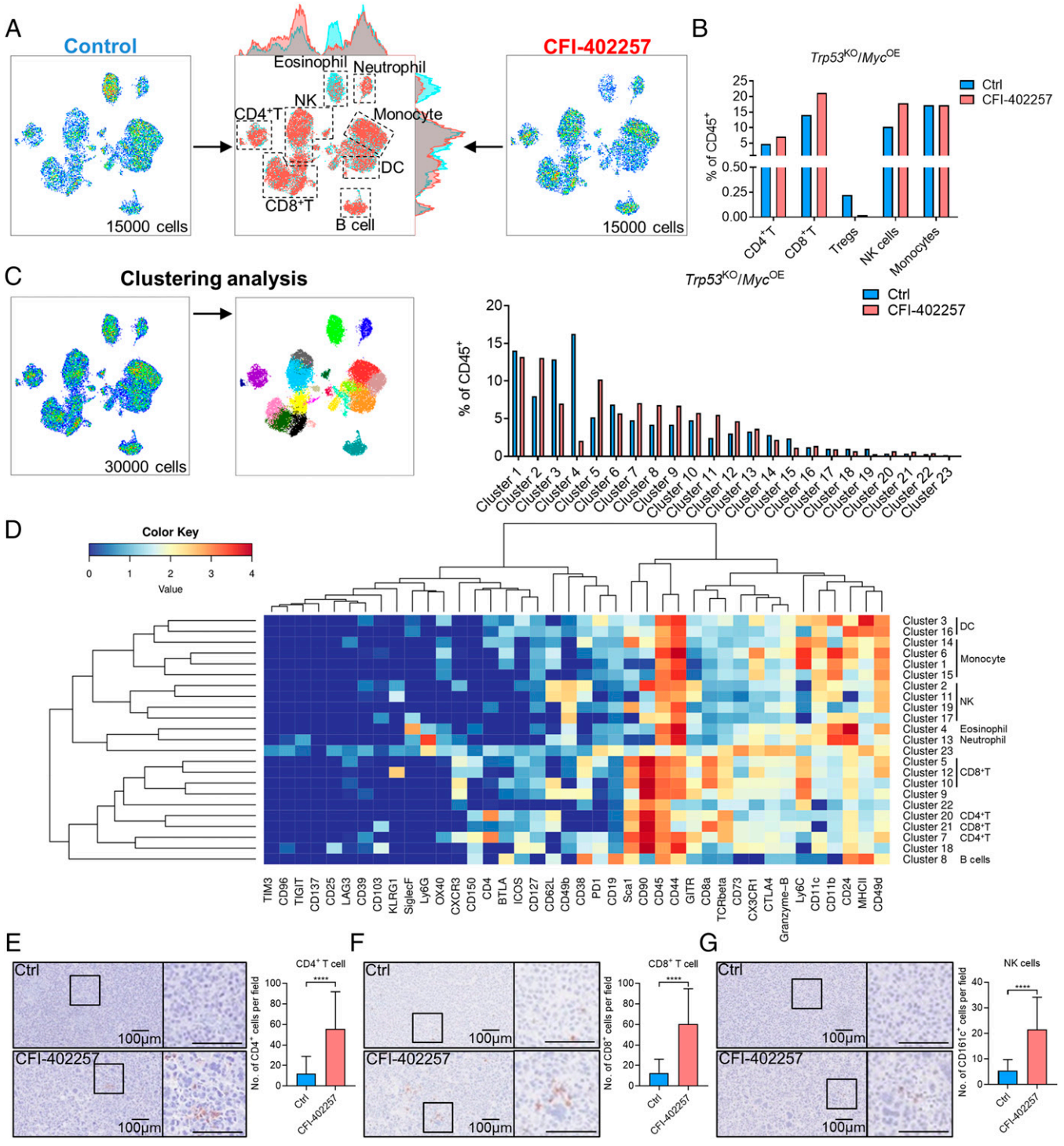

Fig. 6. TTK inhibitor promoted immune surveillance. (*A–D*) Mass cytometry analysis showed the distribution of infiltrated CD45$^+$ cells in *Trp53*^{KO}/*Myc*^{OE} background tumors of HCC-bearing mice (induced by HDTVi), given or not given CFI-402257 treatment. (*A*) UMAP overlay of CD45$^+$ cells presented in HCC tumors. Immune cells types were classified. (*B*) Percentage of different immune cell types. (*C*) Phenograph analysis of CD45$^+$ cells showed 23 clusters were present. Percentage of clusters was calculated. (*D*) Heatmap presenting features of the 23 clusters identified in (*C*), with markers for classification and functional status. (*E–G*) HCC-bearing mice (induced by HDTVi) with *Trp53*^{KO}/*Myc*^{OE} background were treated with 6 mg/kg/day CFI-402257 for 21 d. Tumors were harvested for IHC staining for counting of different immune subsets, HCC regions were shown. (*E*) CD4$^+$ T. (*F*) CD8$^+$ T. (*G*) NK cells. Student's *t* test. $*P < 0.05$, $**P < 0.01$, $***P < 0.001$, $****P < 0.0001$.

checkpoint inhibitor, prolonged survival. Our findings strongly support the future development of CFI-402257 as an anti-cancer therapeutic in HCC.

TTK, the key regulator of SAC, is upregulated in HCC and many other cancers with solid tumors (Fig. 1*E* and *SI Appendix*, Fig. S1), suggesting it as a therapeutic target for these cancers. Aneuploidy is a hallmark of cancer and it was observed in ∼90% solid tumor types, inclusive of breast, pancreatic, and liver cancers (34, 35). Whereas compromised SAC gives rise to aneuploidy and malignant transformation because it permits erroneous mitotic progression and chromosome segregation, it was observed that the aneuploid cancer cells have a seemingly functional SAC (36, 37). It suggests altered SAC functioning may be important for cancer cell survival and protection from further detrimental effects of

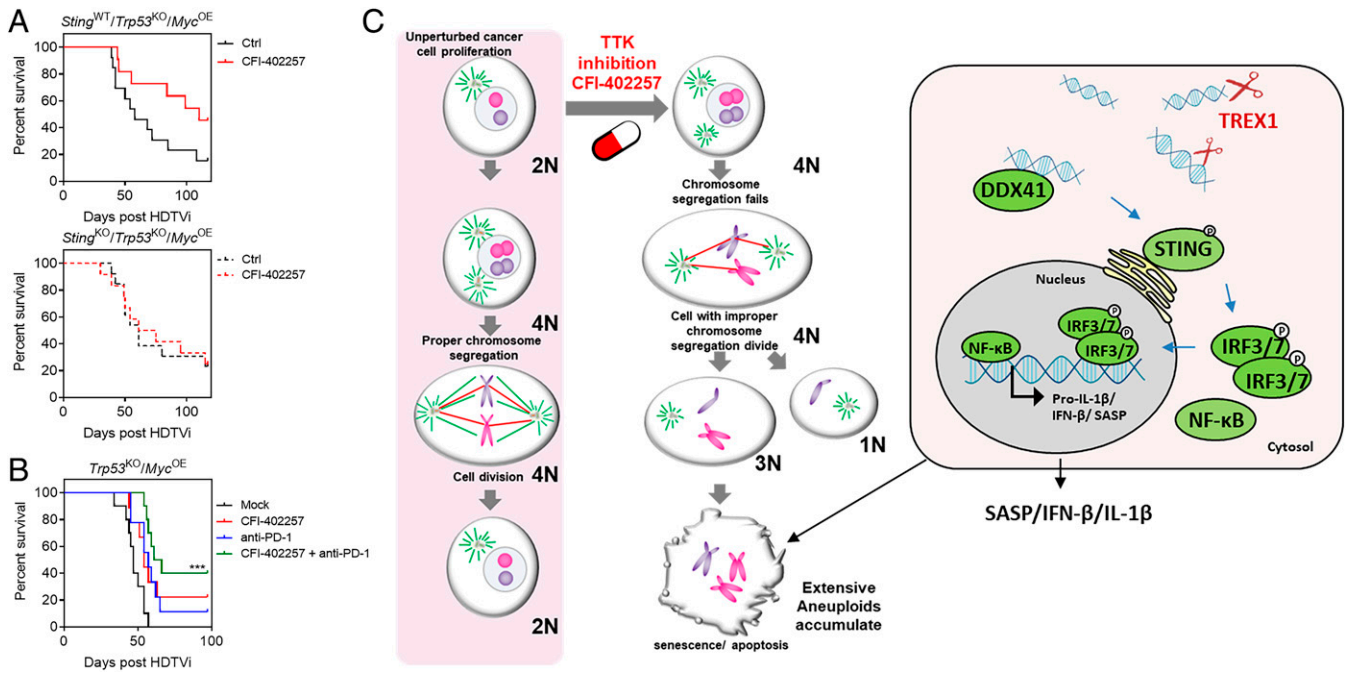

Fig. 7. TTK inhibitor prolonged survival through STING and worked synergistically with anti-PD-1. (*A*) Percentage survival of HCC-bearing mice (induced by HDTVi) with *Sting*$^{WT/KO}$/*Trp53*^{KO}/*Myc*^{OE} background treated with vehicle control (Ctrl) or 6 mg/kg/day CFI-402257. Median days of survival of *Sting*^{WT} groups are 58 (Ctrl) and 110 (CFI-402257). Median days of survival of *Sting*^{KO} groups are 61 (Ctrl) and 68 (CFI-402257). (*B*) Percentage survival of HCC-bearing mice (induced by HDTVi) with *Trp53*^{KO}/*Myc*^{OE} background treated with vehicle control (Ctrl), 6 mg/kg/day CFI-402257 o.g. alone, 10 mg/kg anti-PD-1 i.p. mAb alone, or combination of CFI-402257 and anti-PD-1 mAb. Median days of survival of the four groups (Ctrl, CFI-402257, anti-PD-1, or CFI-402257 + anti-PD-1) are 47, 54, 57, and 63.5, respectively. o.g., oral gavage; i.p., intraperitoneal injection. (*C*) Graphical summary: TTK inhibitor, CFI-402257, blocks proper chromosome segregation by inhibiting spindle assembly checkpoint, resulting in cells with incorrect chromosome number. After several rounds of division, HCC cells with extensive poly/aneuploidy undergo senescence, secreting senescence-associated secretory phenotypes such as CCL2 to recruit immune cells to the site. CFI-402257 deregulates cell cycle, leads to chromosome mis-segregation in HCC cells, and increases cytosolic DNA which is sensed by DDX41 to elicit SASP secretion through STING pathway.

chromosomal instability (CIN) and aneuploidy. Our study revealed that disruption of SAC by targeting TTK using CFI-402257 can induce more severe aneuploidy and effectively suppress HCC proliferation in vitro and in vivo. In fact, in cancer cells, excessive CIN increases its vulnerability against chemotherapy and irradiation (38). Drugs that induce extensive CIN are especially effective in suppressing cancer cells with deranged SAC (21, 39). Although how TTK regulates SAC is still yet to be clarified, its importance in moderating SAC has been shown in many research studies (40). Since the discovery of CIN, aneuploidy has become an attractive target for elimination of cancer cells. In fact, it was shown that TTK inhibitor is an effective anti-cancer agent to suppress growth of aneuploid tumors (18, 41, 42). Our study provided a strategy to target aneuploidy in HCC, by using small molecule inhibitor which binds TTK.

We have shown in our in vivo experiments that HCC tumors with p53 deletion were sensitive to CFI-402257 treatment (Fig. 3*D*). In fact, among HCC patients, p53 mutation/deletion is common and correlated with TTK overexpression (Fig. 1*G*). p53 was known to be a tumor suppressor through inducing cell cycle arrest and apoptosis (43). A study pointed out that p53 protected cells from aneuploidy. p53 was stabilized and activated during prolonged mitotic arrest in SAC and it also activated postmitotic checkpoints (44). Another study using breast cancer model carrying chromosome instability demonstrated that a panel of SAC genes (including TTK) were upregulated but not downregulated or mutated (45). Together, these might suggest a compensatory mechanism of p53 and SAC proteins in maintaining ploidy, as p53 is essential in activating postmitotic checkpoints. Under p53 depletion, SAC genes might be overexpressed to promote cell-cycle arrest and counteract p53 deficiency by preventing mitotic slippage of cancer cells after chromosome mis-segregation. PTEN, another tumor suppressor, mutation/deletion which also correlated with TTK overexpression (Fig. 1*G*), might affect HCC sensitivity toward CFI-402257 similarly, as it also prevents aneuploidy formation by activating multiple checkpoints (46, 47). Our data which showed TTK overexpression in p53/PTEN mutated/deleted human HCC might support the clinical relevance and therapeutic value of CFI-402257 in this cancer type.

Activated STING was found in dimerized form (27). In our study, except dimerization, we also observed an increase in STING monomer protein (Fig. 5*C*), as well as STING mRNA expression level (*SI Appendix*, Fig. S20) after 96 h of CFI-402257 treatment, meaning that STING is upregulated at transcriptional level. A previous study on RIG-I-STING pathway showed the same observation on STING in cells after viral infection. The authors suggested that the transcriptional upregulation of STING might promote a sustained signaling of the pathway, therefore leading to a sustained release of proinflammatory cytokines to fight against virus (48).

Our study identified a mechanism to promote anti-tumor immunosurveillance by using a SAC inhibitor targeting TTK. CFI-402257 activated transcriptional program of SASPs in HCC cells through DDX41-STING cytosolic DNA sensing, which constitute a panel of chemokines and cytokines that attract and activate immune cells. Our transcriptome sequencing data provided us a broader understanding of these upregulated SASPs. Some examples include IL-1α, which promotes neutrophil infiltration, and IL-1β that recruits macrophages and activates dendritic cells (DCs) (49, 50). IL-6 supports B-cell immunoglobulin G (IgG) production (51). It also promotes CD4$^+$ T cells differentiation to

Th17 cells, and $CD8^+$ T cell differentiation to cytotoxic T cells, while inhibiting Treg differentiation (52). CCL2 is a major chemokine for monocytes/macrophages infiltration and promotes Th2 cell development (53, 54). MMP-1 facilitates NK cell migration (55). The properties of these highly induced SASPs suggested their roles in regulating the infiltration of different immune cells. Interestingly, we observed increased NK populations in tumor after CFI-402257 treatment in mass cytometry analysis, and these NK cells represented one of the largest immune populations in tumor, thus our data suggested the importance of NK cells in clearing the tumor cells. ICAM-1 and CXCL5, two SASPs important for NK cell immunosurveillance, were found upregulated after TTK inhibition in our study (56, 57). In a KRAS-mutant lung cancer model, it was shown that the combination of FDA-approved mitogen-activated protein kinase (MAPK) and cyclin-dependent kinase 4/6 inhibitors activated SASPs transcription in tumor cells mediated by retinoblastoma (RB) protein to harness NK cells for tumor clearance (56). At the same time, our study demonstrated that CFI-402257 was able to trigger senescence in HCC cells as a single agent, upregulate NK and T cells activating SASPs (e.g., CCL2, ICAM-1, and IL-6) and other proinflammatory SASPs through cytosolic DNA sensing pathway, and increase immune cells including NK and T cells infiltration to suppress tumor growth. Our data suggested the potential of CFI-402257 as a senescence inducing agent to induce anti-cancer immunity.

There are two mechanistic explanations for the promising combinatorial effects of CFI-402257 and anti-PD-1 treatment. First, as mentioned above, CFI-402257 elicits the SASP program to recruit a variety of immune cells. Anti-PD-1 is able to reactivate the tumor-infiltrated T cells. Second, it was suggested that type 1 interferon pathway upregulated in innate immunity might also activate PD-L1 transcription (58). We showed that combination with anti-PD-1, a currently approved first-line therapy for HCC patients, exhibited improved efficacy to prolong the survival of mice with HCC. This combination may be translated to human HCC patients. Our findings also echo with the synergistic effect found in STING agonists and ICIs. MSA-2 acts as a STING agonist by binding to the cyclic dinucleotides (CDNs) binding pocket of STING dimers (59). Combination of MSA-2 and anti-PD-1 prolonged survival in a MC38 mouse tumor (colon carcinoma) model (59). SR-717, another STING agonist, was found to increase the number of $CD8^+$ T in tumor and enhance their cytotoxicity (60). CFI-402257 has several advantages over STING agonists. Unlike CFI-402257, most of the CDN-based STING agonists undergoing clinical trials are not orally active and have to be administered intratumorally (59, 61). CFI-402257 has dual tumor-suppressive mechanisms including direct inhibition of HCC cell-cycle progression and proliferation and indirect activation of the STING pathway.

In summary, our study reported the efficiency and mechanisms of CFI-402257, a SAC inhibitor targeting TTK, in suppressing HCC. CFI-402257 directly induced apoptosis and indirectly activated DDX41-STING cytosolic DNA pathway to upregulate the transcription program of SASPs and promote immunosurveillance for further tumor clearance. We also demonstrated the potential of CFI-402257 in combination with anti-PD-1 in treating human HCC. Anti-PD-1 and anti-PD-L1 have only been recently approved by FDA as one of the few HCC treatments, our findings are therefore highly clinically relevant. CFI-402257 represents an exciting therapeutic option for advanced HCC patients as single and combined therapeutic agents for HCC.

Materials and Methods

Detailed descriptions of the following methodologies are included in supplementary methods: use of patient samples, HCC cell lines and cell culture, establishment of knockdown and overexpression clones using HCC cell lines, animal studies, quantitative real-time PCR (qPCR), preparation of single-cell suspension from HCC tumors, flow cytometry analysis, mass cytometry/CyTOF analysis, transcriptome sequencing and data analysis, cell proliferation assay, immunofluorescent staining, immunohistochemistry staining, Western blotting, ELISA, senescence-associated β-galactosidase (SA-β-Gal) staining, quantification of cytosolic DNA, and statistical analysis. We thank the Imaging and Flow Cytometry Core, Centre for PanorOmic Sciences (CPOS) in the University of Hong Kong for providing the facilities in this study.

Data Availability. Patient data from online TCGA database was retrieved from cBioPortal website http://www.cbioportal.org/. All transcriptome sequencing data are available in NCBI Sequence Read Archive (SRA) system (PRJNA859195). All other data supporting findings of this study are available in this article and *SI Appendix*.

ACKNOWLEDGMENTS. This work was supported by a Croucher Innovation Award, The University of Hong Kong-Outstanding Young Researcher Award, and the National Natural Science Foundation of China (NSFC) (81974433).

Author affiliations: [a]Department of Pathology, The University of Hong Kong, Pok Fu Lam, Hong Kong Island, Hong Kong; [b]Department of Diagnostic Radiology, The University of Hong Kong, Pok Fu Lam, Hong Kong Island, Hong Kong; [c]Department of Medicine, The University of Hong Kong, Pok Fu Lam, Hong Kong Island, Hong Kong; [d]State Key Laboratory of Liver Research, The University of Hong Kong, Pok Fu Lam, Hong Kong Island, Hong Kong; [e]The Campbell Family Institute for Breast Cancer Research, Princess Margaret Cancer Centre, Toronto, ON, Canada; and [f]Centre for Oncology and Immunology, Hong Kong Science Park, Hong Kong

Author contributions: C.Y.-K.C., T.W.M., and C.C.-L.W. contributed concept and design of this study; C.Y.-K.C., D.K.-C.C., V.W.-H.Y., C.-T.L., B.P.-Y.W., J.W.-S.C., D.L., A.P.-W.T., M.S.Z., and K.V.T. analyzed and interpreted data; C.Y.-K.C. and C.C.-L.W. drafted the manuscript; K.L.T., D.W.C. and I.S.-B. contributed to important intellectual content; C.Y.-K.C. and C.-T.L. performed statistical analysis; C.C.-L.W. contributed funding acquisition and project administration; A.P.-W.T. and K.V.T. provided technical support; I.O.-L.N. provided human HCC tissues; P.-L.K., T.C.-C.Y., M.R.B., T.W.M. and C.C.-L.W. provided material support; T.W.M., and C.C.-L.W. supervised this study.

Reviewers: G.F., University of California San Diego; and A.L., Tisch Cancer Institute.

1. M. Ikeda *et al.*, Safety and pharmacokinetics of lenvatinib in patients with advanced hepatocellular carcinoma. *Clin. Cancer Res.* **22**, 1385–1394 (2016).
2. J. M. Llovet *et al.*; SHARP Investigators Study Group, Sorafenib in advanced hepatocellular carcinoma. *N. Engl. J. Med.* **359**, 378–390 (2008).
3. R. S. Finn *et al.*; IMbrave150 Investigators, Atezolizumab plus bevacizumab in unresectable hepatocellular carcinoma. *N. Engl. J. Med.* **382**, 1894–1905 (2020).
4. S. J. Casak *et al.*, FDA approval summary: Atezolizumab plus bevacizumab for the treatment of patients with advanced unresectable or metastatic hepatocellular carcinoma. *Clin. Cancer Res.* **27**, 1836–1841 (2020).
5. J. Bruix, "Regorafenib shows significant survival gains in refractory liver cancer" in *European Society for Medical Oncology (EMSO) Congress, World Congress on Gastrointestical Cancer* (2016).
6. A. B. El-Khoueiry *et al.*, Nivolumab in patients with advanced hepatocellular carcinoma (CheckMate 040): An open-label, non-comparative, phase 1/2 dose escalation and expansion trial. *Lancet* **389**, 2492–2502 (2017).
7. C. Dominguez-Brauer *et al.*, Targeting mitosis in cancer: Emerging strategies. *Mol. Cell* **60**, 524–536 (2015).
8. A. Musacchio, E. D. Salmon, The spindle-assembly checkpoint in space and time. *Nat. Rev. Mol. Cell Biol.* **8**, 379–393 (2007).
9. S. Kilpinen, K. Ojala, O. Kallioniemi, Analysis of kinase gene expression patterns across 5681 human tissue samples reveals functional genomic taxonomy of the kinome. *PLoS One* **5**, e15068 (2010).
10. X. D. Liang *et al.*, Expression and function analysis of mitotic checkpoint genes identifies TTK as a potential therapeutic target for human hepatocellular carcinoma. *PLoS One* **9**, e97739 (2014).
11. B. A. Tannous *et al.*, Effects of the selective MPS1 inhibitor MPS1-IN-3 on glioblastoma sensitivity to antimitotic drugs. *J. Natl. Cancer Inst.* **105**, 1322–1331 (2013).
12. R. Colombo *et al.*, Targeting the mitotic checkpoint for cancer therapy with NMS-P715, an inhibitor of MPS1 kinase. *Cancer Res.* **70**, 10255–10264 (2010).
13. K. D. Tardif *et al.*, Characterization of the cellular and antitumor effects of MPI-0479605, a small-molecule inhibitor of the mitotic kinase Mps1. *Mol. Cancer Ther.* **10**, 2267–2275 (2011).
14. M. Jemaà *et al.*, Characterization of novel MPS1 inhibitors with preclinical anticancer activity. *Cell Death Differ.* **20**, 1532–1545 (2013).
15. R. Laufer *et al.*, Discovery of 4-(4-aminopyrazolo[1,5-a][1,3,5]triazin-8-yl)benzamides as novel, highly potent and selective, orally bioavailable inhibitors of tyrosine threonine kinase, TTK. *Bioorg. Med. Chem. Lett.* **26**, 3562–3566 (2016).
16. Y. Liu *et al.*, Discovery of pyrazolo[1,5-a]pyrimidine TTK inhibitors: CFI-402257 is a potent, selective, bioavailable anticancer agent. *ACS Med. Chem. Lett.* **7**, 671–675 (2016).
17. E. A. Foley, T. M. Kapoor, Microtubule attachment and spindle assembly checkpoint signalling at the kinetochore. *Nat. Rev. Mol. Cell Biol.* **14**, 25–37 (2013).

18. J. M. Mason *et al.*, Functional characterization of CFI-402257, a potent and selective Mps1/TTK kinase inhibitor, for the treatment of cancer. *Proc. Natl. Acad. Sci. U.S.A.* **114**, 3127–3132 (2017).
19. D. K. Chiu *et al.*, Hepatocellular carcinoma cells up-regulate PVRL1, stabilizing PVR and inhibiting the cytotoxic T-cell response via TIGIT to mediate tumor resistance to PD1 inhibitors in mice. *Gastroenterology* **159**, 609–623 (2020).
20. P. Lara-Gonzalez, F. G. Westhorpe, S. S. Taylor, The spindle assembly checkpoint. *Curr. Biol.* **22**, R966–R980 (2012).
21. C. L. Rieder, H. Maiato, Stuck in division or passing through: What happens when cells cannot satisfy the spindle assembly checkpoint. *Dev. Cell* **7**, 637–651 (2004).
22. S. F. Bakhoum *et al.*, Chromosomal instability drives metastasis through a cytosolic DNA response. *Nature* **553**, 467–472 (2018).
23. A. Basit *et al.*, The cGAS/STING/TBK1/IRF3 innate immunity pathway maintains chromosomal stability through regulation of p21 levels. *Exp. Mol. Med.* **52**, 643–657 (2020).
24. M. De Cecco *et al.*, L1 drives IFN in senescent cells and promotes age-associated inflammation. *Nature* **566**, 73–78 (2019).
25. A. Takahashi *et al.*, Downregulation of cytoplasmic DNases is implicated in cytoplasmic DNA accumulation and SASP in senescent cells. *Nat. Commun.* **9**, 1249 (2018).
26. S. R. Paludan, A. G. Bowie, Immune sensing of DNA. *Immunity* **38**, 870–880 (2013).
27. J. Kwon, S. F. Bakhoum, The cytosolic DNA-sensing cGAS-STING pathway in cancer. *Cancer Discov.* **10**, 26–39 (2020).
28. Z. Zhang *et al.*, The helicase DDX41 senses intracellular DNA mediated by the adaptor STING in dendritic cells. *Nat. Immunol.* **12**, 959–965 (2011).
29. M. Ruscetti *et al.*, Senescence-induced vascular remodeling creates therapeutic vulnerabilities in pancreas cancer. *Cell* **181**, 424–441.e21 (2020).
30. F. J. Hartmann *et al.*, Comprehensive immune monitoring of clinical trials to advance human immunotherapy. *Cell Rep.* **28**, 819–831.e4 (2019).
31. V. Lennerz *et al.*, The response of autologous T cells to a human melanoma is dominated by mutated neoantigens. *Proc. Natl. Acad. Sci. U.S.A.* **102**, 16013–16018 (2005).
32. A. N. Houghton, J. A. Guevara-Patiño, Immune recognition of self in immunity against cancer. *J. Clin. Invest.* **114**, 468–471 (2004).
33. D. K. Chiu *et al.*, Hepatocellular carcinoma cells up-regulate PVRL1, stabilizing PVR and inhibiting the cytotoxic T-cell response via TIGIT to mediate tumor resistance to PD1 inhibitors in mice. *Gastroenterology* **159**, 609–623 (2020).
34. U. Ben-David, A. Amon, Context is everything: Aneuploidy in cancer. *Nat. Rev. Genet.* **21**, 44–62 (2020).
35. A. M. Taylor *et al.*; Cancer Genome Atlas Research Network, Genomic and functional approaches to understanding cancer aneuploidy. *Cancer Cell* **33**, 676–689.e3 (2018).
36. S. L. Thompson, D. A. Compton, Examining the link between chromosomal instability and aneuploidy in human cells. *J. Cell Biol.* **180**, 665–672 (2008).
37. A. Tighe, V. L. Johnson, M. Albertella, S. S. Taylor, Aneuploid colon cancer cells have a robust spindle checkpoint. *EMBO Rep.* **2**, 609–614 (2001).
38. S. F. Bakhoum, L. C. Cantley, The multifaceted role of chromosomal instability in cancer and its microenvironment. *Cell* **174**, 1347–1360 (2018).
39. Y. Cohen-Sharir *et al.*, Aneuploidy renders cancer cells vulnerable to mitotic checkpoint inhibition. *Nature* **590**, 486–491 (2021).
40. Z. Dou *et al.*, Dynamic localization of Mps1 kinase to kinetochores is essential for accurate spindle microtubule attachment. *Proc. Natl. Acad. Sci. U.S.A.* **112**, E4546–E4555 (2015).
41. K. L. Thu *et al.*, Disruption of the anaphase-promoting complex confers resistance to TTK inhibitors in triple-negative breast cancer. *Proc. Natl. Acad. Sci. U.S.A.* **115**, E1570–E1577 (2018).
42. L. Zheng *et al.*, Tyrosine threonine kinase inhibition eliminates lung cancers by augmenting apoptosis and polyploidy. *Mol. Cancer Ther.* **18**, 1775–1786 (2019).
43. J. Chen, The cell-cycle arrest and apoptotic functions of p53 in tumor initiation and progression. *Cold Spring Harb. Perspect. Med.* **6**, a026104 (2016).
44. C. Vogel, A. Kienitz, I. Hofmann, R. Müller, H. Bastians, Crosstalk of the mitotic spindle assembly checkpoint with p53 to prevent polyploidy. *Oncogene* **23**, 6845–6853 (2004).
45. B. Yuan *et al.*, Increased expression of mitotic checkpoint genes in breast cancer cells with chromosomal instability. *Clin. Cancer Res.* **12**, 405–410 (2006).
46. B. H. Choi, S. Xie, W. Dai, PTEN is a negative regulator of mitotic checkpoint complex during the cell cycle. *Exp. Hematol. Oncol.* **6**, 19 (2017).
47. A. Radu, V. Neubauer, T. Akagi, H. Hanafusa, M. M. Georgescu, PTEN induces cell cycle arrest by decreasing the level and nuclear localization of cyclin D1. *Mol. Cell. Biol.* **23**, 6139–6149 (2003).
48. Y. Liu *et al.*, RIG-I-mediated STING upregulation restricts herpes simplex virus 1 infection. *J. Virol.* **90**, 9406–9419 (2016).
49. P. Rider *et al.*, IL-1α and IL-1β recruit different myeloid cells and promote different stages of sterile inflammation. *J. Immunol.* **187**, 4835–4843 (2011).
50. T. Luft *et al.*, IL-1 beta enhances CD40 ligand-mediated cytokine secretion by human dendritic cells (DC): A mechanism for T cell-independent DC activation. *J. Immunol.* **168**, 713–722 (2002).
51. K. Maeda, H. Mehta, D. A. Drevets, K. M. Coggeshall, IL-6 increases B-cell IgG production in a feed-forward proinflammatory mechanism to skew hematopoiesis and elevate myeloid production. *Blood* **115**, 4699–4706 (2010).
52. T. Tanaka, M. Narazaki, T. Kishimoto, IL-6 in inflammation, immunity, and disease. *Cold Spring Harb. Perspect. Biol.* **6**, a016295 (2014).
53. S. L. Deshmane, S. Kremlev, S. Amini, B. E. Sawaya, Monocyte chemoattractant protein-1 (MCP-1): An overview. *J. Interferon Cytokine Res.* **29**, 313–326 (2009).
54. S. A. Luther, J. G. Cyster, Chemokines as regulators of T cell differentiation. *Nat. Immunol.* **2**, 102–107 (2001).
55. S. Goda *et al.*, Matrix metalloproteinase-1 produced by human CXCL12-stimulated natural killer cells. *Am. J. Pathol.* **169**, 445–458 (2006).
56. M. Ruscetti *et al.*, NK cell-mediated cytotoxicity contributes to tumor control by a cytostatic drug combination. *Science* **362**, 1416–1422 (2018).
57. Y. Nie, M. C. Jiang, C. Liu, Q. Liu, X. Zhu, CXCL5 has potential to be a marker for hepatocellular carcinoma prognosis and was correlating with immune infiltrates. *Front. Oncol.* **11**, 637023 (2021).
58. N. Jacquelot *et al.*, Sustained type I interferon signaling as a mechanism of resistance to PD-1 blockade. *Cell Res.* **29**, 846–861 (2019).
59. B. S. Pan *et al.*, An orally available non-nucleotide STING agonist with antitumor activity. *Science* **369**, eaba6098 (2020).
60. E. N. Chin *et al.*, Antitumor activity of a systemic STING-activating non-nucleotide cGAMP mimetic. *Science* **369**, 993–999 (2020).
61. J. Le Naour, L. Zitvogel, L. Galluzzi, E. Vacchelli, G. Kroemer, Trial watch: STING agonists in cancer therapy. *OncoImmunology* **9**, 1777624 (2020).